Available online at www.sciencedirect.com
ScienceDirect
Journal of Power Sources 164 (2007) 397–414
JOURNAL OF POWER SOURCES
www.elsevier.com/locate/jpowsour

Review

Thermal activated (thermal) battery technology Part II. Molten salt electrolytes

Patrick Masset [a,*], Ronald A. Guidotti [b]

[a] *Karl Winnacker Institut der Dechema e.V., Theodor-Heuss Allee 25, 60486 Frankfurt am Main, Germany*
[b] *Sierra Nevada Consulting, 1536 W. High Pointe Ct. Minden, NV 89423, USA*

Received 31 March 2006; received in revised form 24 September 2006; accepted 24 October 2006
Available online 1 December 2006

Abstract

This article gives an overview of the important properties and design characteristics of electrolyte used in thermally activated (thermal) batteries. The basic physical properties of the main compositions are reviewed. The properties of electrolytes such as melting point, ionic conductivity, surface tension, density, thermal characteristics, and moisture sensitivity were analyzed in relation with the functioning of the batteries. Solubility data of alkali metals, sulphides, and oxides were compiled and analyzed. The important parameters of separator pellets are discussed in terms of both electrical and mechanical properties as they pertain to thermal-battery design and functioning. A number of lower-melting electrolytes are presented along with key physical properties for possible use in applications requiring lower operating temperatures such as borehole power supplies.

Keywords: Thermal batteries; Molten salts; Electrolyte

Contents

* Corresponding author. Tel.: +49 697 564 362; fax: +49 697 564 388.
E-mail address: masset@dechema.de (P. Masset).

0378-7753/$ – see front matter © 2006 Elsevier B.V. All rights reserved.
doi:10.1016/j.jpowsour.2006.10.080

1. Introduction

Thermally activated (thermal) batteries are mainly used for military purposes that require a high level of confidence. Applications and the electrochemistry of such power sources were described in detail in the first part of this review dedicated to thermal batteries [1]. The knowledge of the physical and chemical phenomena arising from the components should be well known and understood to master the global functioning of such complex systems. This article is focused on molten salts used as electrolytes in thermal batteries. The electrolytes suitable for use in thermal batteries require certain properties and are selected according the following criteria:

- low vapor pressure: the electrolyte should not evaporate inside the battery;
- high ionic conductivity: very important for "pulse" (high-rate) applications;
- large electrochemical window: i.e., no chemical reaction between the electrode materials and electrolyte constituents:

o no oxidation of the electrolyte by the cathode materials,
o no reduction of the electrolyte by anode materials,

- low or no solubility of Li_2O: it modifies the electrolyte retention properties of the separator:

o electrolyte leakage can occur, resulting in "soft" shorts between cells in the battery stack,

- low solubility of elemental Li and Li-alloy anodes: this decreases the efficiency of the cells by electronic conduction in the molten salt;
- low solubility of the cathode and anode materials: minimizes self-discharge reactions with attendant loss in capacity;
- low solubility of discharge products: minimizes possible self-discharge reactions;
- stable towards moisture and/or oxygen: prevents the production of hydroxides and/or oxides in the molten salt;
- compatible melting point: lower than the thermal decomposition temperatures of the electrode materials;
- ability to wet the binder in the separator and the electrodes: minimizes the contact resistance at the electrolyte (separator)/electrode interface.

All these points are discussed in this review. Available data in the open literature were analyzed. The key conclusions are given for the Li-alloy/FeS_2 system. However, insights on electrolytes used in other technologies are briefly described. The first section describes the main basic properties of the single salts or mixtures. The following sections are devoted to issues encountered with the use of high-temperature molten salts in batteries.

2. Lithium-halide electrolytes

Lithium halide-based mixtures were mainly used for their low melting points (compared to sodium halide mixtures), low vapor pressure, their relative high ionic conductivities. Fig. 1 shows the phase diagrams of the main electrolytes used or envisioned for use in thermal batteries. The molar and mass compositions of the main electrolytes are listed in Table 1.

Those compositions taken from the literature [2–27] are now considered as accurate and are well accepted. Most of these phase diagrams were optimized to determine the excess mixing properties (see Refs. [9,28] for the binary systems and ternary systems, respectively). The choice of the electrolyte is usually dictated by the envisioned application and the shape of the phase diagram may be relevant. Using the LiCl–KCl eutectic compositions precipitation phenomena were observed in the anode compartment (LiCl precipitation) and in the cathode compartment (KCl precipitation) for high current densities [29]. Braunstein and Vallet described the concentration profiles of Li^+ and K^+ along the electrolyte for Li/LiCl–KCl/S type-generator [30]. It is mainly ascribed to the difference in transport number of the two cations Li^+ and K^+ in the LiCl–KCl eutectic. This might be avoided, but not entirely suppressed, by the use of all-lithium electrolytes. The second alternative is the use of multi-cation electrolyte with a low liquidus slope (dT/dx), e.g., the ternary LiCl–LiBr–KBr eutectic. The precipitation of salt in the tortuosity of the electrodes partially blocks the electrode/electrolyte interface and reduces the electrochemical active surface. The overall cell resistance increases and the expected battery voltage cannot be realized. Usually, the temperature range of functioning for a given electrolyte is empirically fixed at m.p. + 50 °C to avoid the precipitation phenomena.

2.1. Electrochemical window

The electrochemical window is one of the main features of the electrolytes because it fixes the limits of the cathodic and

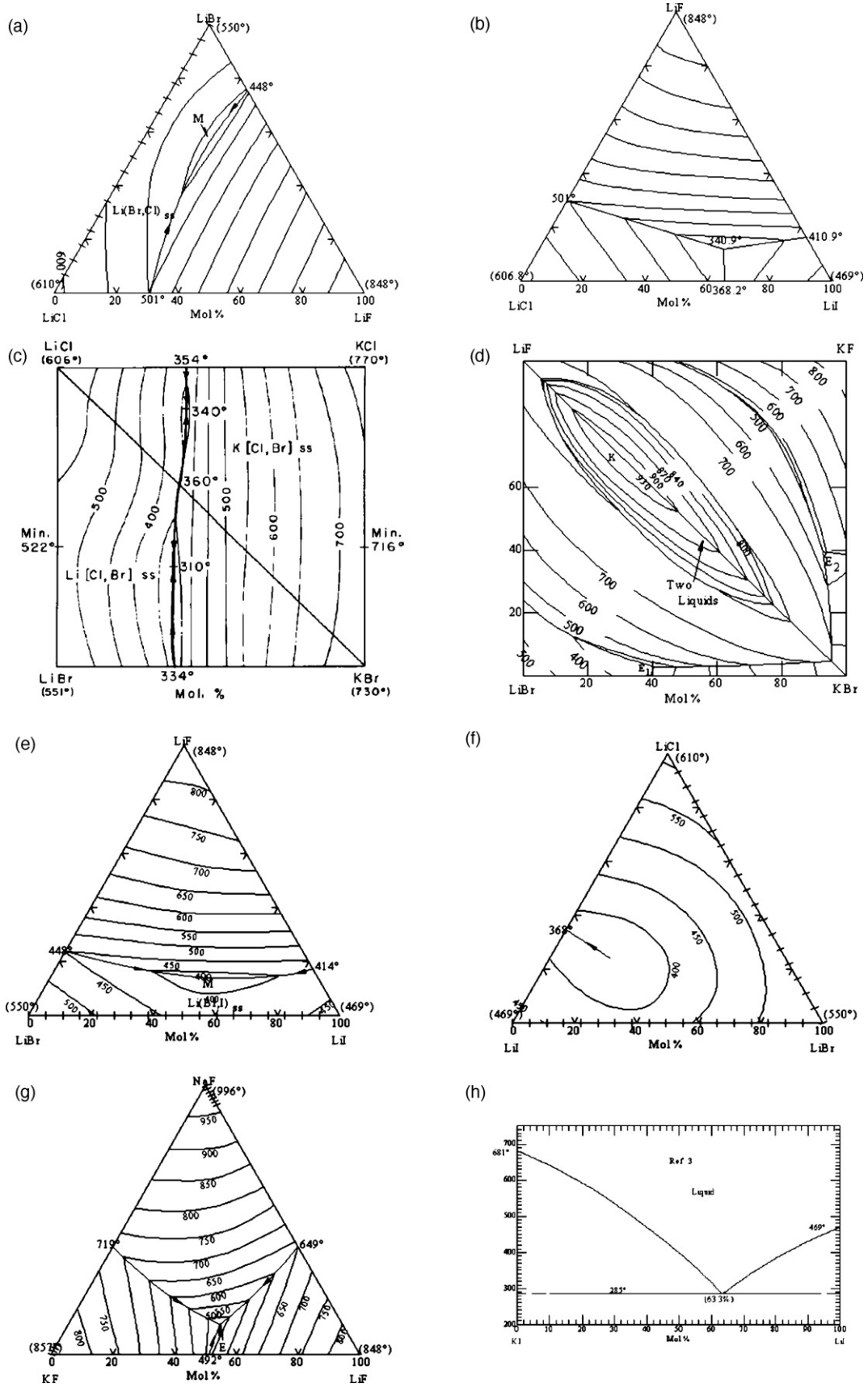

Fig. 1. Phase diagrams of selected electrolytes: (a) LiF–LiCl–LiBr from Ref. [2], (b) LiF–LiCl–LiI from Ref. [7], (c) LiBr–LiCl–KBr–KCl, (d) LiBr–LiF–KBr–KF, (e) LiBr–LiF–LiI from Ref. [8], (f) LiBr–LiCl–LiI from Ref. [8], (g) LiF–NaF–KF from Ref. [13], (h) LiI–KI from Ref. [9].

Table 1
Melting point and composition of some electrolytes

Electrolyte	Composition (mass%)	Composition (mol%)	m.p. (°C)
LiCl–KCl	44.8–55.2	58.8–41.2	354 [4], 352 [9]
LiBr–KBr	52.26–47.74	60–40	320 [9]
LiI–KI	58.2–41.8	63.3–36.7	285 [4], 260 [9–11], 280 [12], 285,286 [9]
LiF–LiI	3.7–96.3	16.5–83.5	410.9 [17]
LiBr–LiF	91.4–8.6	76–24	448 [18]
LiCl–LiI	14.4–85.6	34.6–65.4	368 [9]
LiF–LiCl	21.2–78.8	30.5–69.5	501[9]
LiF–LiCl–LiBr	9.6–22–68.4	22–31—47	443 [2], 436 [3], 444 [4], 430 [19]
LiF–LiBr–KBr	0.67–53.5–45.83	0.67–53.5–45.83	324 [4], 323 [5]
	0.81–56–43.18	3–63–34	312 [6]
		3.5–54.5–42	320 [15]
LiCl–LiBr–KBr	12.05–36.54–51.41	25–37–38	310 [20–22], Tt [8]
LiF–NaF–KF	29.5–10.9–59.6	46.5–11.5–42	455 [13]
LiCl–KCl–LiF	53.2–42.1–4.7	62.7–28.8–9.1	397 [23]
LiCl–KCl–LiBr	42.1–42.8–15.1	57–33–10	416 [23]
LiCl–KCl–NaCl	42.63–48.63–8.74	61.2–29.7–9.1	429 [23]
LiCl–KCl–LiI	44.2–45.0–10.7	57–33–10	394 [23]
LiCl–KCl–KI	37.6–51.5–10.9	54–42–4	367 [25]
LiBr–LiCl–LiI	19–24.3–56.7	16.07–10.04–73.88	368 [8]
LiF–LiCl–LiI	3.2–13–83.8	11.7–29.1–59.2	341 [4,7,17]
LiCl–LiI–KI	2.6–57.3–40.1	8.5–59–32	265 [14], 264 [24]
LiF–LiCl–LiBr–LiI	4.9–11.2–34.9–49	15.4–21.7–32.9–30	360 [11]
	5.0–19.6–22.6–52.8	14.7–35.5–20–29.8	318–326 [19]

anodic potentials. This decomposition window is very temperature dependent, which can be quite important since thermal batteries operate at elevated temperature. Fig. 2 shows the temperature dependence of the decomposition potentials for lithium halides based on theoretical thermodynamic data [31].

The cathodic limit is given by the reduction potential of the least stable cation in the mixture, whereas, the anodic limit corresponds to the oxidation potential of the least stable anion. Thermodynamic values for single salts have already been published and are compared with experimental values for mixtures. In molten salt, the stability of the cation ranges from Rb > Cs > K > Na > Li. In mixtures containing several cations, lithium is the easiest alkali metal to reduce. This is the reason why cesium cannot be recovered by electrolysis in Li-containing alkali halides mixture by pyrochemical process for the reprocessing of nuclear fuels. At the other extremity of the potential scale, the fluorides are the most stable halides: F > Cl > Br > I. The critical point is the high redox potential of sulfur-based species, e.g., in Li–Al/FeS_2 batteries, regarding the less stable halide iodide. The oxidation potential of iodide is 3.14 V versus Li^+/Li at 450 °C (723 K) [32]. In iodide-based mixtures, it was measured to be close to 2.55 V versus Li–Si reference at 425 °C (698 K), which is around 1 V lower than with pure chloride-based electrolytes [33]. At 460 °C (733 K), the redox potentials of the pyrite-base system, dissolved polysulfides and polysulfites are close to 1.95, 2.35 and 2.5 versus Li–Si [34], respectively. It means the electrolyte is stable with the Li–Si/FeS_2 couple whatever the halide is in the electrolyte mixture. Oxide- and hydroxide-base redox systems are located in the electrochemical window [35,36]. From an electrochemical point of view, the presence of residual oxides or hydroxides in the electrolyte, coming from the hydrolysis of the salt, does not interfere directly with the electrolyte itself but auto-discharge reactions may be envisaged by direct reaction of dissolved oxide with the pyrite.

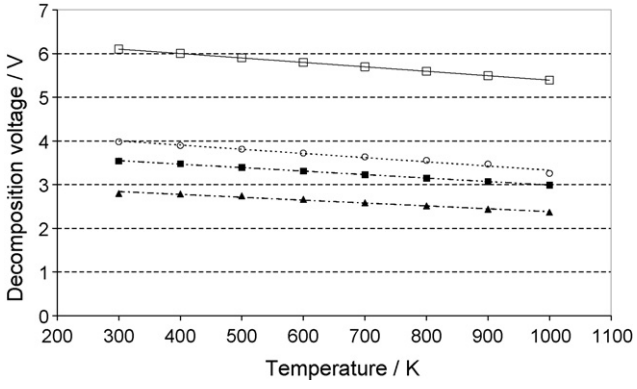

Fig. 2. Thermodynamic decomposition potentials for halides of lithium (data from Ref. [31]), (□) LiF, (◯) LiCl, (■) LiBr, (▲) LiI.

2.2. Ionic conductivity

As ionic media, molten salts exhibit rather high ionic conductivities (1–5 S cm^{-1}) regarding ionic liquids: (1–10) × 10^{-3} S cm^{-1} [37]) or solid electrolytes: 10^{-6} to 10^{-2} S cm^{-1} at 700 °C (973 K) [38]. In molten salts, "current" transportation through single cells is ensured by the ionic species migration. Usually, their mobility follows Arrhenius-type behavior. In Table 2, the resulting ionic conductivity is expressed as follows

Table 2
Ionic conductivity of selected electrolytes

Electrolyte	Composition (mass%)	Ionic conductivity (S cm^{-1})	Value at 475 °C	References
LiCl–KCl	58.8–41.2	18.7876 exp(−1800.6/T (K))	1.69 1.57 at 450 °C	[39] [11]
LiI–KI	58.2–41.8	10.0001 exp(−1387.9/T (K))	1.56 2.24 at 607 °C	[39] [41]
LiCl–LiI	14.4–85.6	13.0462 exp(−907.3/T (K))	3.88	[39]
LiF–LiCl–LiBr	9.6–22–68.4	17.8664 exp(−1284.24/T (K))	3.21	[39]
LiF–LiBr–KBr	0.67–53.5–45.83	20.5817 exp(−1944.76/T (K))	1.56	[39]
	0.81–56–43.18	23.021 exp(−16204.9)/RT (K))	1.75	[44]
LiCl–LiBr–KBr	12.05–36.54–57.41	–	1.7	[41]
LiF–LiCl–LiI	3.2–13–83.8	8.895 exp(−872.6/T (K))	2.77 2.3 at 375 °C	[39] [11,40]
LiBr–LiCl–LiI	19–24.3–56.7	12.6746 exp(−925.0/T (K))	3.68	[39]
LiCl–LiI–KI	2.6–57.3–40.1	11.0055 exp(−1329.4/T (K))	1.86	[39]

[39–41]:

$$\kappa = \kappa^0 \exp\left(\frac{E_a}{RT}\right) \quad (1)$$

where κ is the pre-exponential factor, E_a represents the activation energy, R the gas constant ($R = 8.3145$ J mol^{-1} K^{-1}), and T is the absolute temperature. Lithium-based electrolytes exhibit the highest ionic conductivities due the high mobility of the lithium cation compared to other alkali-based electrolytes (Fig. 3). Electrolytes with higher atomic fractions of Li^+ will have higher ionic conductivities. This is readily evident from the data of Fig. 4.

In thermal batteries, due to the high level of mechanical stresses (acceleration, shock, spin, vibration, etc.), the electrolyte must be firmly immobilized by a binder. It constitutes the so-called "separator". Usually, the binder is made of powders of metallic oxides such as silica, alumina or magnesia that are electrical insulators. MgO is the preferred choice as it is thermodynamically stable in contact with high-activity anodes at elevated temperatures. Moreover, its solubility in molten salts remains low even at high temperature: pK(MgO) = 7.2 [42] and 8.38 [43] in the LiCl–KCl eutectic at 450 and 700 °C, respectively. In the NaCl–KCl, Cherignets [43] determined pK(MgO) to be close to 11.62 at 700 °C. It means the solubility of MgO is enhanced in the NaCl–KCl mixture compared to the LiCl–KCl eutectic. Redey et al. [44] measured the ionic conductivities of retained electrolytes (LiCl–KCl, LiCl–LiBr–KBr, LiF–LiCl–LiBr, LiF–LiBr–KBr). They expressed the "ionic conductivity of the separator" as follows:

$$\kappa = \kappa^0 \exp\left(\frac{E_a}{RT}\right) \psi_{MgO}^{\alpha} \quad (2)$$

The parameter ψ_{MgO} represents the mass fraction of magnesia MgO and the parameter α depends on the nature of the electrolyte. Moreover, the free volume remaining after the pelletization step modifies significantly the ionic conductivity of the separator [45]. The conductivity is greatly influenced by the tortuosity of the separator. Conductivities as a function of temperature are presented in Fig. 5 for pellets of a number of common thermal-battery separator materials. As expected, the all-Li separator has the largest conductivity by far, which is why it is the preferred choice for high-power application.

It is important to note that the absolute conductivity of the electrolyte is not the primary design factor to consider. Instead, it is the conductivity of the separator pellet that is

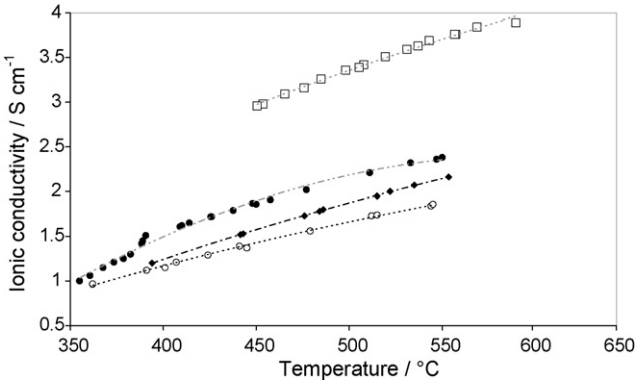

Fig. 3. Ionic conductivities of some common thermal-battery electrolytes as a function of temperature, (□) LiCl–LiBr–LiF Eut., (●) LiCl–LiBr–KBr LiCl-rich:39 m/o LiCl, (♦) LiCl–KCl Eut., (○) LiCl–LiBr–KBr Eut. 25 m/o LiCl.

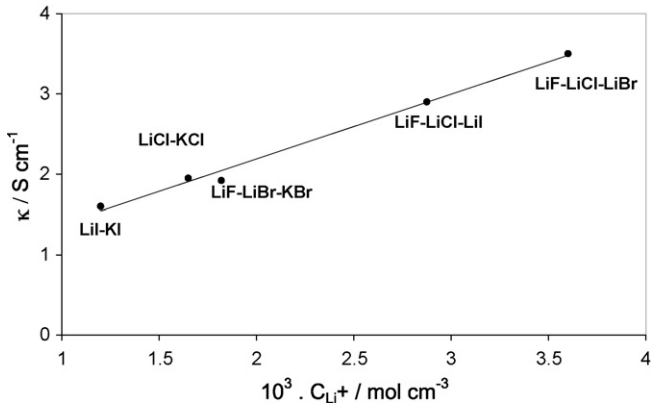

Fig. 4. Ionic conductivity vs. the lithium concentration in the electrolyte (500 °C).

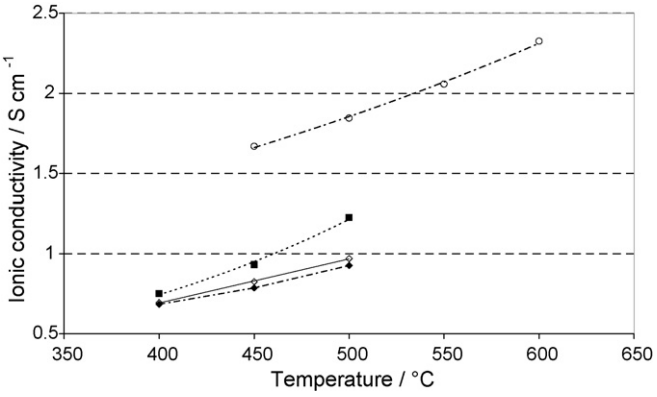

Fig. 5. Ionic conductivities of separator pellets as a function of temperature for select electrolyte compositions, (◊) LiCl–KCl Eut. (35 mass% MgO), (♦) LiCl–LiBr–KBr Eut. (30 mass% MgO), (■) LiBr–KBr–LiF Eut. (25 mass% MgO), (○) LiCl–LiBr–LiF Eut. (35 mass% MgO).

important. Different electrolytes require different amount of a given binder for effective immobilization by capillary action because of the required mechanical properties of the separator at high temperatures when the electrolyte is molten. (This is discussed in detail in Section 4.2.) For example, while 35% MgO is necessary for the LiCl–KCl and LiCl–LiBr–LiF electrolytes, the lower-melting LiBr–KBr–LiF eutectic requires only 25% for equivalent results. The tortuosity and porosity (electrolyte volume fraction) of the separator pellets impacts the final conductivity [46–48]. Modeling of the separator conductivity indicates that percolation theory of the porous structure with a distribution of porosities best fits the experimental data [45].

2.3. Density

The density of the single salts and mixtures are of importance during the design step where the volume and the mass are critical parameters. Values found in the literature [49–53] are grouped in Table 3. It should be pointed out that the density in the liquid state is somewhat 20–25% lower than in the solid state [49]. It may lead to an over-pressure in the stack during the heating phase after battery activation and cause electrolyte leakage. Usually, the density of the mixture increases with the size of the anion involved in the mixture. It might be detrimental in the process design where the mass parameter is crucial. However, the ratio ρ(cr.) over ρ(liq.) for bromide- or iodide-based mixtures remains constant in the range 1.2–1.25 as for chloride mixtures.

Table 3
Summary of the literature values of liquid salt densities ρ(liq.) at 500 °C and solid salt densities ρ(cr.) at 25 °C

Electrolyte	ρ(cr.) (g cm^{-3})	ρ(liq.) (g cm^{-3})
LiCl–KCl	2.01 [49]	1.59 [49], 1.6 [50]
LiI–KI	3.53 [49]	2.83 [49], 2.77 [53]
LiF–LiCl–LiBr	2.91 [49], 2.92 [52]	2.17 [49], 2.19 [52]
LiF–LiCl–LiI	3.513 [49]	2.69 [49]

2.4. Surface tension

The surface tension affects the degree of wetting of the binder material by the molten salt, which, in turn, affects the capillary forces acting on the binder. The three-phase region of gas, solid, and liquid is determined by the relative energies involved, as shown in Fig. 6.

This will determine the final contact angle of the liquid on the solid. In the case of the pressed-powder separator materials (MgO), the contact angle will be that of the molten salt. The solid–vapor surface tension, γ_{SV}, reflects the interaction of the solid and gas phases. The liquid–solid vapor tension, γ_{LS}, reflects the interaction of the solid and liquid phases. The liquid–vapor surface tension, γ_{LV}, reflects the interactions of the liquid and vapor phases. The net interaction is defined by Young's equation [54,55]:

$$\gamma_{LV}\cos(\phi) = \gamma_{SV} - \gamma_{SL} \quad (3)$$

The smaller the wetting angle (ϕ), the better the wetting. In the case of separators for thermal batteries, the factors that are relevant are:

- composition of the binder used in the separator (including impurities);
- composition of the molten salt;
- composition of the atmosphere surrounding the sample;
- surface tension of the molten salt;
- temperature;
- pressure (this is important in a real battery);
- shape of the MgO particles;
- origin of the binder (e.g., MgO Maglite "S").

For example, the surface tension of the LiCl–KCl eutectic electrolyte at 823 K is 122 dyne cm^{-1} [56]. This compares to 79.1 dyne cm^{-1} for water at room temperature [57]. If a thermal battery should overheat, the reduced surface tension could result in massive electrolyte leakage because of dewetting from the binder. This can result in breaching of the separator, leading to shorting between the anode and cathode that can cause a thermal runaway that destroys the battery. Wetting angle of MgO by molten LiCl–KCl eutectic was experimentally measured [33,58]. The LiCl–KCl eutectic presents a good wetting behavior on MgO surface (wetting angle of 56° [33] and 60° [58] at 450 °C). In contrast, the pyrite FeS_2 is poorly wetted by the molten LiCl–KCl eutectic. The wetting angle was found to be close to 120 °C [33,58]. The wetting behavior of MgO and FeS_2 is depicted in Fig. 6 [33]. The wetting behavior (decrease of the wetting angle) is also enhanced by the presence of dissolved oxides [33]. The solubility of lithium oxide in LiCl was measured in LiCl [59] and calculated for the purposes of pyrochemical process [60,61]. In the NaCl–KCl system, Barbin and Nekkrasov [62] determined the solubility of Li_2O to be $S_{Li_2O}^{NaCl-KCl} = (0.187–5.221) \times 10^{-3}/T$ (K). This latter value agrees with the previous determination made by Kaneko and Kojima [63] who estimated the solubility of Li_2O in NaCl–KCl to be close to 0.31 mol% at 700 °C. Despite the solubility of

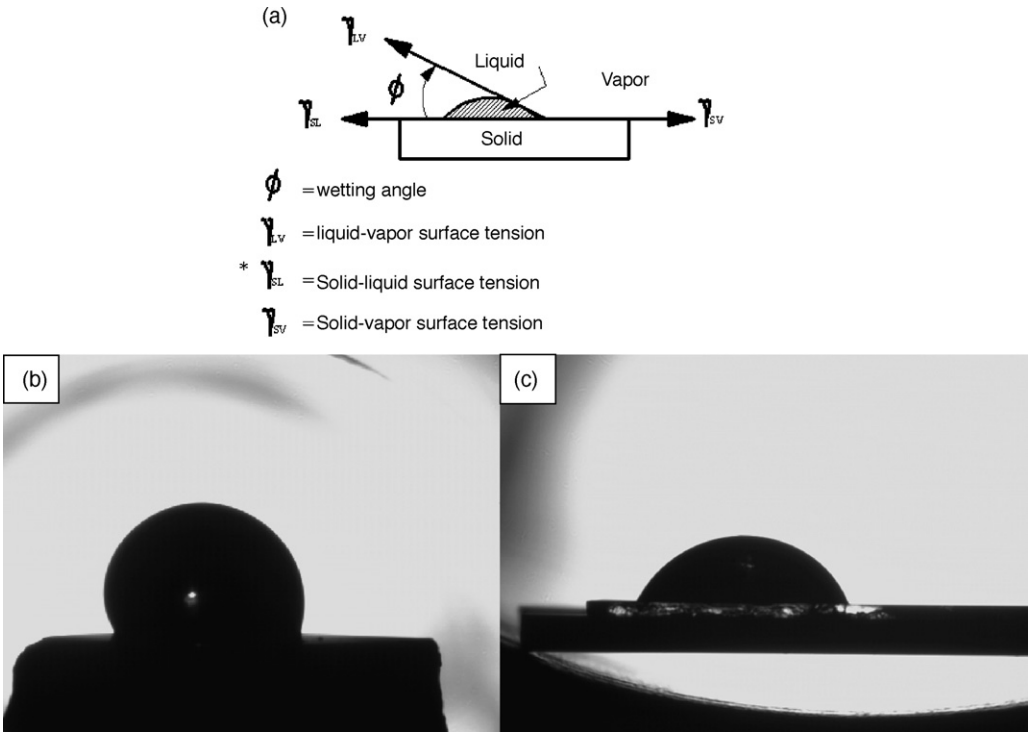

Fig. 6. (a) Schematic representation of the wetting of a solid by a liquid phase, (b) wetting angle of the LiCl–KCl eutectic on pyrite FeS_2 substrate in Ar–H_2 5 (v/o), (b) wetting angle of the LiCl–KCl eutectic on MgO ⟨1 1 1⟩ substrate in Ar–H_2 5 (v/o).

oxides in molten salts (lower than 1 mol% in the LiCl–KCl) it may modify significantly the electrolyte retention properties. It has been shown to cause electrolyte leakage and may induce soft short between cells in the stacks. It should be also mentioned that lithium oxide (Li_2O), as well as lithium sulfide Li_2S, are used in the catholyte as anti-peak (lithiation) agent to remove the potential peak (voltage spike) arising from oxidized species in the earlier stage of the battery discharge.

2.5. Thermal properties

Heat management is critical for the proper functioning of a thermal battery. Information regarding the thermal properties of the battery constituents (viz., cathode, anode, separator, and pyrotechnic) is necessary for the design of the battery to determine the amount of insulation required and the amount of heat necessary for a given application. The most important thermal properties are the heat capacity of the electrolyte in the solid and molten states C_p(cr.) and C_p(liq.), respectively, and the heat of fusion ΔH_f. The heat capacity of the mixture can be evaluated according to the below equation:

$$C_p(T) = \sum_i X_i C_{p,i}(T) \quad (4)$$

where X_i is the molar fraction of constituent i and $C_{p,i}(T)$ is the heat capacity of the constituent i versus the temperature. Values of heat capacities of single salts are reported in Table 4. However,

Table 4
Heat capacity C_p(cr.) and C_p(liq.) (J K^{-1} g^{-1}) and heat of fusion ΔH_{fusion} (J g^{-1}) of the single salts [26]

Salt	C_p(cr.) (J K^{-1} g^{-1})	C_p(liq.) (J K^{-1} g^{-1})	ΔH_{fusion} (J g^{-1})
LiF	2.389	3.613	59.6
LiCl	2.744	3.545	26.8
LiBr	2.794	3.911	11.6
LiI	2.844	3.776	6.25
KF	4.471	3.814	26.7
KCl	2.930	4.111	20.1
KBr	2.988	4.173	12.2
KI	3.015	3.944	9.15

Table 5
Heat capacity C_p (J K^{-1} g^{-1}) and heat of fusion ΔH_{fusion} (J g^{-1}) of the electrolytes

Salts	$C_p(T_f)$ (J K^{-1} g^{-1})	$\Delta C_p = C_p$(liq.) − C_p(cr.) (J K^{-1} g^{-1})	ΔH_{fusion} (lit.) (J g^{-1})
LiCl–KCl	0.74	0.26	244 [33], 234.78 [64]
LiI–KI	0.55	0.85	71 [33]
LiF–LiCl–LiBr	0.87	0.41	266 [33], 293.80 [64]
LiF–LiCl–LiI	1.22	ND	157 [33]
LiF–LiBr–KBr	0.505	0.248	103 [33], 134 [64]

the heat capacities of mixtures have to be measured because the melting point of the eutectic compositions and single salts are often different. This limits the determination of the heat capacity of the electrolyte over the full temperature range of interest. The heat capacities of a number of electrolytes have already been determined and the literature data [33,64] are summarized in Table 5.

3. Hygroscopicity of salts

3.1. $MX{\cdot}nH_2O$ hydrates (M = Li, Na, K and X = F, Cl, Br, I)

Alkali halides are known to be sensitive to moisture. It was shown that the water up-take kinetic follows the order: iodide > bromide > chloride ≈ fluoride in a dry-room at <3% RH [65]. These results are in agreement with previous measurement performed by Redey et al. [5] who estimated that the water uptake rate by LiF–LiBr–KBr eutectic was eight times higher than that for the LiCl–KCl eutectic due to the high hygroscopicity of LiBr. Moreover, it was pointed out that the kinetic constant was multiplied by a factor of 10 when the water partial pressure was multiplied by three. The sensitivity towards moisture decreases from Li to Na, K alkali. No hydrate forms between sodium and potassium halides as well as LiF and water at room temperature. In the case of KCl, the $KCl{\cdot}H_2O$ phase was established by several authors [66–69]. A continuous equilibrium exists between KCl and H_2O. In contrast, lithium salts are known to form $LiX{\cdot}nH_2O$ (X = F, Cl, Br, I) hydrates [33,70–74] (see Fig. 7). Water is taken up as water of crystallization. The value of n varies from 1 to 3 depending on the anion. The thermal stability of the hydrates depends on the number of waters of hydration present, the nature of the anion X, and the partial pressure of water (see Fig. 8, example of DTA/TG curves obtained with $LiCl{\cdot}H_2O$). The decomposition temperatures of $LiX{\cdot}nH_2O$ hydrates (X = Cl [33,70,71,72], Br [33,70,71], I [33,73,74]) have been measured by thermal analysis under inert gas (see Table 6).

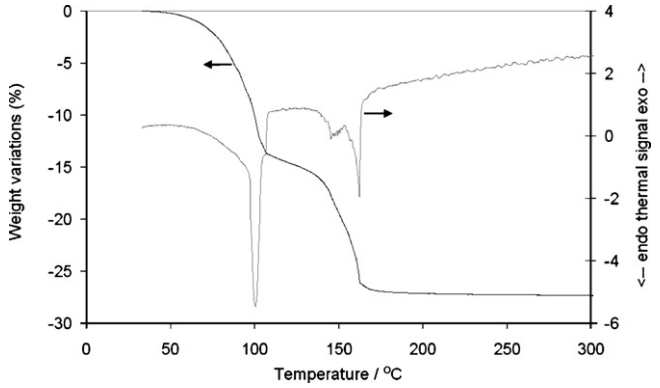

Fig. 8. Typical DTA/TGA spectra recorded at 1 °C min^{-1} under helium atmosphere of the $LiCl{\cdot}H_2O$ hydrate.

In the case of lithium halides (e.g., LiCl and LiBr), work at Sandia has shown that the water uptake is completely reversible, with the water being completely removed by vacuum drying overnight at 125–150 °C. This is not the case for $MgCl_2{\cdot}6H_2O$, however, where MgO and HCl are formed on electrolyte melting. It disagrees with the calculated phase diagram (Fig. 7) given by Zeng [69] who used the experimental data of several authors which evidenced four successive hydrates in the $MgCl_2$–H_2O system: $MgCl_2{\cdot}6H_2O$ [66,75], $MgCl_2{\cdot}4H_2O$ [66,76], $MgCl_2{\cdot}2H_2O$ [66,76], $MgCl_2{\cdot}H_2O$ [77] to give $MgCl_2$ in equilibrium with H_2O at high temperature).

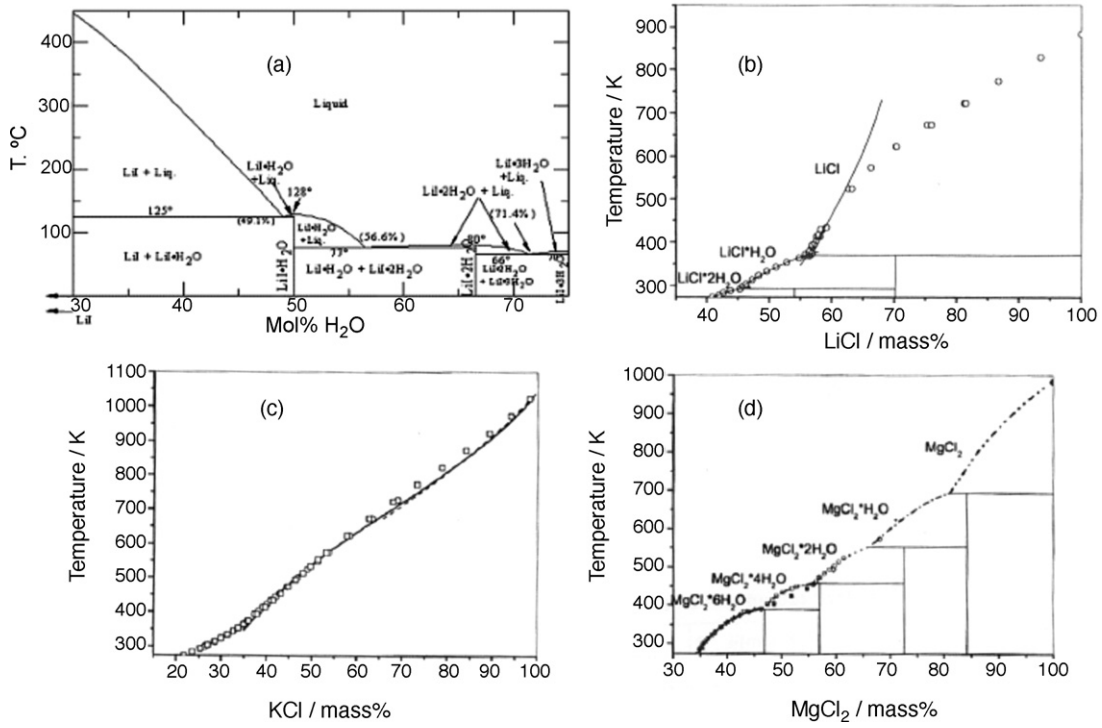

Fig. 7. Phase diagrams of MX–H_2O systems: (a) LiI–H_2O [73], (b) LiCl–H_2O [69], (c) KCl–H_2O [69], (d) $MgCl_2$–H_2O [69].

Table 6
Decomposition temperature of $LiX{\cdot}nH_2O$ hydrates (X = Cl, Br, I) under inert atmosphere by thermal analysis

Hydrate	$T_{experimetal}$ (°C)
$LiCl{\cdot}H_2O$	98 [33], 110 [70], 100.5 [71], 99 [72]
$LiCl{\cdot}(1/2)H_2O$	160 [33], 162 [70], 152 [71]
$LiBr{\cdot}H_2O$	159 [71], 160 [70]
$LiBr{\cdot}(1/2)H_2O$	175 [33], 165 [70]
$LiI{\cdot}3H_2O$	210 [70]
$LiI{\cdot}H_2O$	190 [33]
$LiI{\cdot}(1/2)H_2O$[a]	215 [70]

[a] This compound was observed by Chevalier [74], whereas, Rudo et al. [73] denied its existence.

3.2. Drying procedures

A drying step has to be carried out before the salt processing to remove adsorbed or crystallized water and to avoid hydrolysis of the salt during heating. It means that the drying temperature should be above the decomposition temperature of the most stable hydrate (see Table 6). It should be pointed out that the dehydration of the salt depends also on the partial pressure of water above the salt. If a vacuum is applied during the drying process, the drying temperature can be lowered. The highest temperature should correspond to the temperature where the reaction between the salt and the moisture occurs.

In the literature, it was noted that LiI was successfully dried in 8 h between 200 and 230 °C under vacuum without hydroxide formation [78], whereas, Kleppa extended the drying step over two weeks with a temperature ramp up to the melting point [79]. By DTA measurements carried out with a known amount of water in salt contained in a sealed crucible, the hydrolysis temperatures of LiBr and LiI were found to be 371 and 326 °C, respectively [4]. This is in good agreement with the eutectic temperature of the LiBr-LiOH and LiI–LiOH mixtures [80]. Moreover, the re-crystallization temperature of the mixture obtained was found to be close to the liquidus temperature predicted by the phase diagram of the salt–hydroxide mixture. According to the LiF–LiOH [81] and LiCl–LiOH [9] phase diagrams, the eutectic temperatures are 431 and 314 °C, respectively.

The hydrolysis of the LiCl–KCl eutectic was determined to be close to 250 °C by Parash et al. [82]. This agrees well with the eutectic temperature of 262 °C proposed for the eutectic for the reciprocal system LiCl–LiOH–KCl–KOH [83]. Regarding the previous studies devoted to the drying of salts, the drying step should be carried out in a temperature window between 200 and 250 °C and under vacuum over a sufficient long time to allow diffusion of residual water. After vacuum drying for 16 h at 125 °C, the water content of LiCl–KCl eutectic ranges from 0.05 to 0.07 (w/o) [84].

4. Retention of the electrolyte

Due to the high level of environmental stresses (acceleration, spin, shock, and vibration) that the thermal battery can encounter during operation, the molten electrolyte must be stabilized or retained by capillary forces in a binder (e.g., MgO).

4.1. Binder

In the past, ceramic fiber felts were used to immobilize the electrolyte. A BN felt was developed by Argonne National Laboratory for use in its secondary battery program [85,86]. This was abandoned in favor of an oxide powder, since anodes and cathodes are manufactured using powder technology. A considerable effort was mounted at Sandia National Laboratories in the 1970s to develop alternative binders to the kaolin clay that was then being used for Ca/LiCl–KCl/$CaCrO_4$ thermal batteries [87]. Fumed silica (SiO_2) was found to work quite well, was inexpensive, and required only a small amount (10 mass%) to get an acceptable electrolyte immobilization comparable to the kaolin clay that needed 30–40%. (This material is formed by the steam hydrolysis of $SiCl_4$.) The large number of surface functions, groups on the SiO_2 surface explain the low level of binder required. A number of fumed silicas and fumed titania and alumina were examined for possible use as binders. The latter oxides did not work as well as the silicas and required 50–100% more material for equivalent binding action [52]. Silica was eventually abandoned because of its high reactivity with metallic lithium and lithium-alloy anodes at the elevated temperatures during thermal-battery operation. Inert oxide such as Y_2O_3, ZrO_2, and others inert materials such as BN have also been examined.

An extensive investigation was conducted of the properties of magnesia (MgO), the most commonly used electrolyte binder, to determine the most important ones for good electrolyte immobilization [88]. Different parameters were investigated such as magnesia type (source), particle size and morphology, BET surface, chemical impurities, pore-size distribution, and calcining temperatures. The various MgOs were formulated into separator mixes that were then characterized so that their properties could be correlated with those of the MgO. The main conclusions were that only the pore-size distribution and morphology could be tied to the MgO that performed the best (Maglite 'S'). This material had a bimodal particle-size distribution and a unique pore-size distribution that provided the necessary capillarity for effective electrolyte immobilization. The degree of electrolyte leakage from the separator and the separator deformation were found to be excellent metrics for binder characterization and qualification. (See next section for details.) Excessively high calcination temperatures (>700 °C) resulted in sintering of the MgO particles that adversely affected the pore-size distribution and, consequently, the immobilization capability (Table 7).

Table 7
Summary of the optimum volume and weight fractions Ψ_{MgO} of magnesia

	LiCl–KCl	LiF–LiBr–LiCl	LiI–KI	LiF–LiCl–LiI
Ψ_{MgO} (wt.%) [51]	35	30	35	32.5
Ψ_{Mg} (vol.%) [49]	23.3	25.4	30.3	27

4.2. Mechanical properties of the separator

The mechanical properties of the separator are just as important as its electrochemical properties. A high ionic conductivity is of little value if separator pellets cannot be made that are robust and can be handled without cracking or breaking during battery-stack assembly. The properties at battery operating temperatures, when the electrolyte is molten, are equally important. Batteries are closed and welded off under a high-applied pressure (typically, 1.2–2.5 MPa) to maintain good interfacial contact between the pellets in the battery stack and to prevent movement during any environmental stresses while functioning.

Once the electrolyte melts, however, a rapid stack relaxation occurs, with the pressure dropping to <0.4 MPa within seconds [89]. This occurs through deformation of the separator pellet, which is evidenced by a decrease in thickness. This does not occur with the anode and cathode pellets, as the particle sizes of the electroactive materials are relatively large and the particles tend to interlock. Empirically, it has been determined that separator pellet deformation in the range of 15–30% is ideal for thermal batteries during operation. Lower values result in reduced interfacial contact between pellets in the battery stack; much higher deformation leads to separator extrusion into the battery wrap, which can result in excessive electrolyte leakage and possible separator breaching. A number of factors influence the deformation process for a given electrolyte, including temperature, porosity, binder content, and applied pressure [51]. The porosity and binder levels have the most effect, followed by applied pressure.

If the separator pellets are too dense, there is no place for the electrolyte to go once molten, which leads to electrolyte leakage into the ceramic blanket with which the battery stack is wrapped. This can then lead to parasitic shunting currents. (Porosities of 25–30% are found to be ideal.) Techniques for measurement of electrolyte leakage have been developed as part of separator-characterization studies and good correlation was obtained with pellet-deformation behavior [88,90]. These two metrics are very useful when examining a new potential electrolyte for use in thermal batteries. Together, they determine the minimum amount of binder that is necessary to effectively immobilize the electrolyte when used in the separator. Similarly, these can be used to qualify alternative binder materials for use in the separator. The manner in which the electrolyte is blended with the binder can also impact the final properties of the separator pellet, due to particle–particle interactions and grinding action [90]. There will always be a tradeoff between the electrochemical performance (e.g., resistivity) and mechanical requirements of the separator for severe environments. The latter may require increasing the level of binder, which will lead to an increase in the resistance of the separator and a resulting rise in battery impedance.

In contrast to the separator, pressing of the anode and cathode pellets to high densities (<15% porosity) does not affect performance significantly. The higher densities result in thinner pellets and a shorter battery stack, which increases the overall energy density of the battery. However, if the non-malleable Li–Si anodes are over pressed without added electrolyte, radial cracking can occur due to stresses built up in the pellet. The addition of 15–20% electrolyte greatly reduces (by a factor or four or more) the pressure needed to fabricate Li–Si anodes [84].

5. Solubility phenomenon in molten salts

5.1. Solubility of lithium and electronic conductivity

Alkali-metal solubility in alkali metal halides has several origins and was observed mainly during an electrolysis process using molten salts as electrolytes. Plambeck et al. [91] studied lithium hydride electrolysis in LiCl–KCl eutectic at 375 °C and noted Li and K solubility where metallic lithium was generated at the cathode. It was necessary to use temperatures below 450 °C to avoid the metathesis reaction of the metallic lithium with the potassium chloride.

$$Li^0_{(l)} + K^+ \rightarrow K^0_{(g)} + Li^+ \quad (5)$$

Dark deposits that analyzed as pure K were observed the cool part of the electrochemical cell. In thermal batteries, the lithium comes from either the Li–M (M = Al, Si, B) alloys or the "LAN" anodes (Li immobilized with Fe powder). In the latter, the efficiency remains lower than 80% and dissolution of lithium in the salt phase is suspected to explain the lithium losses.

The metallic lithium solubility in the electrolyte may induce self-discharge due to the native electronic conductivity in the molten salt electrolyte [92]. With the pure salts LiX (X = F, Cl, Br, I), the lithium solubility increase correlates with the halide anion radius [93]. In the LiCl salt, the lithium solubility was measured by several authors [94–97]. However, its solubility does not exceed 1 mol% and remains low compared to other alkali metals in solution their metal halide (up to 10 mol% for Na in NaBr). Haarberg et al. [98,99] studied the electronic conduction in Na halide melts. However, they used Bi electrodes and it has been shown that Na–Bi alloys exhibit solubility of Bi as well as Na in molten salts due to Bi^{3-} formation [100]. The electronic conductivity of the Li–LiCl solutions did not exceed 10^{-2} S cm^{-1} [101,102] and is much smaller for other M–MX solutions (M = Na, K, Cs, Rb and X = F, Cl, Br, I). Liu and Poignet [102] showed that the "F defaults" concentration in the Li–LiCl solutions was two order of magnitude higher than the corresponding M–MX solutions. Recently, Hebant and Picard [103] studied the Li–(LiCl–KCl) interface. They demonstrated that the sub-halide Li_2Cl was thermodynamically stable. This could explain the low solubility of metallic lithium in the molten LiCl–KCl and the low electronic conductivity.

The measured lithium solubility in the LiCl–KCl eutectic is between 1 and 2 mol% [96]. The solubility of Li was also verified by Reynolds et al. as being significant in LiCl–KCl electrolytes [104]. The electronic conductivity increased monotonically with temperature and activity of the Li-alloy anode. These results agreed with those reported earlier by Heus and Egan [105]. This translates into a self-discharge current of 34 μA cm^{-2} at 405 °C, increasing to 200 μA cm^{-2} at 465 °C

for Li–Al anodes [104]. Workers at Argonne National Laboratory studied the self-discharge rates of a Li-alloy anode in LiCl–KCl and LiBr–KBr–CsBr eutectics and reported self-discharge rates in the former of 1.0, 1.4, and 1.9 mA cm^{-2} at temperatures of 395, 415, and 436 °C, respectively [106,107]. The self-discharge rate for the LiBr–KBr–CsBr eutectic was much lower, 0.18 mA cm^{-2} at 415 °C, which shows that the electrolyte composition and the Li activity of the anode have a dramatic influence on the self-discharge process. The self-discharge rates for Li–Al/FeS_2 cells on open circuit were almost 80 times less for Li–Si/FeS_2 cells.

Self-discharge rates of 4.7% per day were calculated for engineering-sized Li–Al/FeS_2 cells, which was attributed to electronic conduction of the LiCl–KCl electrolyte [108]. In the case of Li–Cl_2 cells, the saturation level for dissolved Li was not reached due to the presence of dissolved Cl_2 [109]. The use of Li and Li-alloy anodes is not precluded in thermal batteries despite the reduced efficiency caused by unwanted electronic conductivity in molten salts. This is because thermal batteries are not at temperature for prolonged periods as in the case for high-temperature secondary batteries or commercial electrolysis cells.

5.2. Solubility of sulfur-based species

Mainly three sulfides, Li_2S, FeS_2, $FeS_{1.14}$, are involved in the thermal battery functioning. According to the Fe–S diagram, the thermal stability of the FeS_2 depends on sulfur gas pressure [110,111]. FeS_2 (pyrite) is used as a cathode material in thermal batteries and decomposes at temperature between 550 and 600 °C, depending on purity and particle size [112,113]. It leads to the production of pyrrhotite $FeS_{1.14}$ (Fe_7S_8) and sulfur gas evolution in the molten salt electrolyte as shown by the below equation:

$$7FeS_{2(s)} \rightarrow Fe_7S_{8(s)} + 3S_{2(g)} \quad (6)$$

Work has shown that the rate of decomposition of pyrite is dramatically slowed in the presence of electrolyte [114,115]. The electrolyte that coats the pyrite particles inhibits the loss of gaseous sulfur from the cathode. Kinetic constants in molten salts were found to be approximately three orders of magnitude lower than in helium gas atmosphere [115]. The solubilities as a function of temperature of the various sulfur species in molten LiCl–KCl eutectic are summarized in Table 8 and are plotted in Fig. 9.

By recombination of the dissolved sulfur in the molten salt with dissolved lithium arising from the Li-based alloy anode, the formation of a solid insulating layer of Li_2S is observed in the retained electrolyte along with elemental Fe [116–118]. This can cause battery failure by shorting in very thin separators in secondary batteries that may experience electrolyte migration after prolonged discharge times. This is generally not a problem with conventional thermal batteries.

Table 8
Expression of the solubilities of sulfur (Li_2S, FeS_2, $FeS_{1.14}$) vs. the temperature in the LiCl–KCl eutectic

	$\ln X(M_xS_y)$ (moles fraction)
Li_2S	$(11.077–6.1046) \times 10^3/T$ (K) [119–124]
FeS_2	$(10.753–11.882) \times 10^3/T$ (K) [125]
$FeS_{1.14}$	$(6.4477–7.6622) \times 10^3/T$ (K) [125]

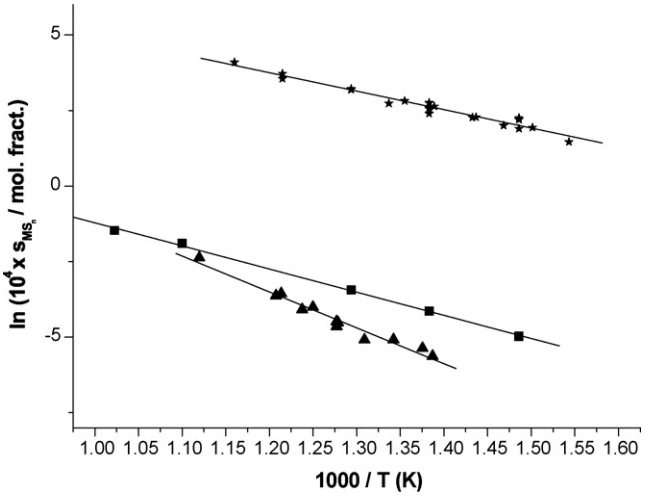

Fig. 9. Logarithm of solubility of Li_2S, FeS_2 and $FeS_{1.14}$ in LiCl–KCl eutectic vs. the inverse of the absolute temperature. (⋆) Li_2S data from Ref. [119–124], (■) FeS_2 from Ref. [126], (▲) $FeS_{1.14}$ from Ref. [126].

The solubilities of Li_2S in the LiCl–KCl eutectic [119–124], FeS_2 [125] and $FeS_{1.14}$ [125] have been experimentally determined. The Li_2S solubility limit was also determined in xLiCl–$(1-x)$KCl mixtures ($0.4 < x < 0.6$) [119,126] and in the LiF–LiCl [123] and LiF–LiCl–LiBr [127] electrolytes, respectively. Santarini [128,129] reported the solubility limit of FeS_2 in the LiCl–KCl eutectic to be 5.28×10^{-4} in molar fraction. This value is lower than the previous values (mean value: 13.7×10^{-4} at 450 °C) in the LiCl–KCl eutectic. It was explained by the formation of the so-call "J-phase" ($LiK_6Fe_{24}S_{26}Cl$) at a temperature below 470 °C described later by Tomczuk et al. [130] arising from the reaction between $FeS_{1.14}$ and the molten chlorides [131,132]. The solubilities of Li_2S, FeS_2, and $FeS_{1.14}$ follow Arrhenius-type law. The analytical expressions are reported in Table 8.

The nature of the sulfur-containing species arising from dissolution of FeS_2 in molten salts has not been totally ascertained. It is know that solutions of elemental sulfur in LiCl–KCl electrolyte give rise to blue colors [133,134]. However, in the case of FeS_2–LiCl–KCl solutions, an amber color is obtained [84]. This may be explained by the presence of polysulfide species that may involve Fe, as shown in the below equation:

$$FeS_{2(s)} \rightarrow Fe^{2+} + S_2^{2-} \quad \text{(polysulfide)} \quad (8)$$

(The sulfur is originally present in FeS_2 in the form of polysulfide [135,136].) The polysulfide may undergo dissociation to form elemental sulfur that can be lost from the melt by evaporation:

$$S_2^{2-} \rightarrow 0.5S_{2(g)} + S^{2-} \quad (9)$$

Or, it can experience oxidation:

$$S_2^{2-} \rightarrow 0.5S_{2(g)} + S^{-} + e^{-} \quad (10)$$

The S^- species has been postulated previously [134]. The chemistry and electrochemistry of S and Fe–S species in complex and not yet completely understood.

In addition, there is the possibility in a conventional thermal cell of direct chemical reaction of the Fe–S solution species with dissolved Li that results from the Li-alloy anode:

$$4Li^0{}_{(soln)} + Fe^{2+} + S_2{}^{2-} \rightarrow Fe^0{}_{(s)} + 2Li_2S_{(s)} \quad (11)$$

This would explain the observation of clusters of particles of Fe and Li_2S found in the separators of deeply discharges Li–Si/FeS_2 cells [114,117]. Nevertheless, it should be emphasized that the reaction between sulfur and sulfide in the molten salt may increase the total solubility of sulfur-based species [137].

Analysis of filtered and quenched aliquots of molten electrolyte equilibrated with FeS_2 indicate that the atomic S/Fe ratio increases dramatically to >5 relative to 2 for the solid pyrite [84]. Loss of S from the electrolyte by volatilization would result in a S/Fe ratio <2. The reduced ratios could indicate that loss of Fe by precipitation may be occurring, as shown in the below equation:

$$Fe^{2+} + S_2{}^{2-} \rightarrow FeS_{(s)} + S^{2-} \quad (11)$$

Data by Sharma and Seefurth show a solubility of FeS_2 in LiCl–KCl electrolyte of 2.51×10^{-6} moles fraction at 550 °C [125]. In contrast, a value of 6.85×10^{-5} moles fraction was determined by Guidotti by direct chemical analysis of an aliquot of the solution filtered at temperature; a S/Fe atomic ratio of 3.28 was noted for the sample [84].

The composition of the electrolyte has a significant affect upon self-discharge, due to differences in the solubility of the various sulfur-containing species arising from the FeS_2 in contact with the melt [117]. The discharge current density and temperature also impact the process, with greater losses occurring at lower current densities and higher temperatures [114]. For example, Li-alloy/FeS_2 cells with an all-Li electrolyte (3.21LiF–13.04LiCl–83.75LiI, m/o) lost capacity of the upper-voltage plateau at the rate of 0.172% per day at 350 °C at discharge rates of 20–60 mA cm^{-2}. This increased to 0.217% per day at 450 °C. When a lower-melting electrolyte (0.95LiCl–5.14LiBr–45.09LiI–16.75KI–32.07CsI, m/o) was used, loss of capacity dropped to 0.05% per day at a rate of 1–5 mA cm^{-2} at 200 °C. (The lower rate was necessitated by the much lower temperature.) When the electrolyte contains K^+, there is the possibility for formation of the J-phase ($LiK_6Fe_{24}S_{26}Cl$). This is one possible reason for some of the loss in capacity of the lower-voltage plateau for the cells using the 12.05LiCl–36.53LiBr–51.42KBr (m/o) electrolyte at >20 mA cm^{-2}. This was not observed for cells with the all-Li electrolyte [114].

6. Lower-melting electrolytes

6.1. Alkali halide systems

Thermal batteries are used as the primary power sources for defense applications and for nuclear weapons. There has been interest in recent years to adapt this technology for possible select domestic applications, such as a power source for borehole drilling application [138–144]. The idea was to eliminate the use of the internal pyrotechnic and use the heat of the borehole to keep the electrolyte molten during use. However, this would require the use of electrolytes that melt ≤300 °C [145–149]. None of the electrolytes listed in Table 1 would be suitable for this application. The incorporation of iodide ions and Rb and Cs cations results in a number of promising candidates; these are listed in Table 9.

Codd reported on the performance of the Li(Al)/FeS_2 couple in single cells based on LiBr–CsBr, LiBr–CsCl, LiBr–RbBr, and LiCl–RbCl eutectics [150]. Under a 3-Ω load, none performed well at 320 °C. At 360 °C, the order of decreasing cell life under the same load was LiBr–CsBr > LiBr–CsCl > LiBr–RbBr ≫ LiCl–RbCl. No batteries were built with these electrolytes.

The performance of the Li–Si/FeS_2 couple with the LiCl–LiBr–LiI–KI–CsI pentanary eutectic has shown reasonable performance in battery stacks at temperatures as low as 200 °C [84]. However, an intrinsic problem at these lower temperatures is the reduced rate capability due to kinetic effects and higher battery impedance because of the increased resistivity of the separator. (The much larger Cs^+ has an intrinsically lower mobility than Li^+.) As a result, sustainable current densities of <5 mA cm^{-2} are typical, which is more than two orders of magnitude less than what is typical for conventional thermal batteries operating at 400 °C or higher. One way to engineer around this is to electrically parallel several battery stacks to share the load (Fig. 10).

The use of iodides would result in a thermal battery that would be somewhat heavier than one based on the LiCl–KCl eutectic

Table 9
Halide eutectics with melting points <300 °C

Electrolyte	Composition (mol%)	Melting point (°C)	Density (g cm^{-3})	Conductivity (cm^{-1})
LiBr–RbBr	42–58	271 [145]	2.63 at 647 °C	1.33 at 567 °C
LiBr–CsCl	42–58	262 [146]	–	2.68 at 800 °C
LiI–KI	40–60	260 [147]	2.57 at 637 °C	2.22 at 607 °C
LiBr–CsBr	59–41	259 [9]	2.82	–
LiCl–KCl–CsCl	57.5–13.3–20.2	265 [25]	2.23	0.28 at 280 °C
LiCl–KCl–RbCl–CsCl	55.5–18.7–1.4–24.3	258 [148]	–	–
LiBr–KBr–CsBr	56.1–18.1–25.3	236 [149]	–	–
LiBr–LiI–KI–CsI	9.6–54.3–16.2–19.9	189 [25]	–	–
LiCl–LiBr–LiI–KI–CsI	3.5–9.2–52.4–15.7–19.2	184 [25], 151 [84]	3.1	–

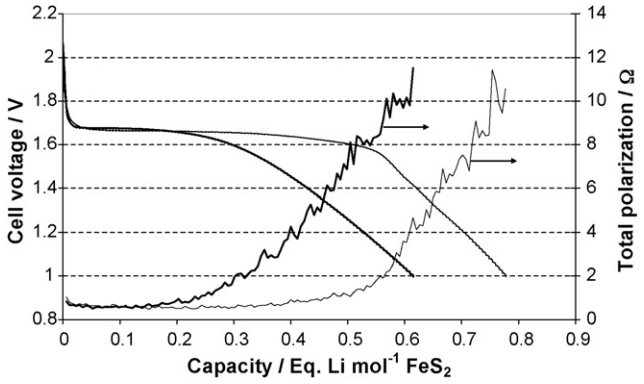

Fig. 10. Comparison of the performance of the Li–Si/FeS_2 couple in LiBr–KBr–CsBr (bold line) and LiCl–LiBr–LiI–KI–CsI (normal line) eutectics in single cells at 250 °C and 8 mA cm^{-2} [84].

due to the higher density of the salt—especially for an all-iodide system. These salts are also more expensive than the bromides and chlorides. (Cs and Rb halides are even more expensive.) In addition, iodide electrolytes suffer from sensitivity towards oxidation by oxygen to form elemental iodine. This occurs even at the low humidities (<3% RH) found in dry rooms. Melting of these salts during electrolyte preparation must be done under an inert atmosphere and the materials stored under similar conditions. This is not practical for the commercial manufacturing of thermal batteries because of the constraints it imposes. In addition, there is evidence of increased self-discharge for batteries using such salts [151].

The Li–Si/FeS_2 couple has also been examined for possible borehole applications using the LiBr–KBr–CsBr eutectic electrolyte that melts at 236 °C [139–141]. While single-cell performance was acceptable, it suffered from similar impedance problems observed with the pentanary iodide electrolyte. The resistivity of the separator was 23.29 Ω cm at 290 °C and 8.22 at 450 °C (30% MgO), which compares to 1.25 Ω cm for the LiCl–LiBr–KBr electrolyte at 450 °C (30% MgO) [20,44,118].

The separator resistivity is the largest contributor to the total polarization, n_{tot}, which can be defined as follows:

$$n_{tot} = n_{actA} + n_{actC} + n_{irA} + n_{irS} + n_{irC} + n_{concA} + n_{concC} \quad (9)$$

where the n_{actA} and n_{actC} refer to activation polarization, n_{irA}, n_{irC}, and n_{irS} refer to ohmic polarization, and n_{concA} and n_{concC} refer to concentration polarization. ("A" refers to the anode, "C" to the cathode, and "S" to the separator). The types and extent of polarization will depend primarily upon the electrochemical system, temperature, current density (which depends on the load and electrode surface area), electrolyte composition, and physical configuration of the cell. Other factors may also be involved in certain situations.

The total polarization can be viewed as a resistance in series with the cell or battery. Obviously, one wants to minimize all possible sources of polarization in any system, to maximize the power that can be delivered. The various types of polarization are discussed briefly below.

6.1.1. Activation polarization

The energy associated with initiation of the charge-transfer process (rate of reaction) at an electrode is defined as the activation energy. The resistance to this transfer process is the activation polarization. This is a kinetically related phenomenon and is generally not relevant for batteries that operate at high temperatures (e.g., >450 °C). However, this can start becoming important at temperatures below 200 °C for borehole applications. The kinetics of the reaction determine how rapidly the reactions can take place—reduction at the cathode and oxidation at the anode. As with all chemical reactions, this type of polarization is very temperature sensitive; it becomes less important at elevated temperatures, where the rates are higher (e.g., in conventional thermal batteries). This type of polarization typically shows Arrhenius behavior.

6.1.2. Ohmic polarization

Ohmic polarization is related the electrical conductivity of the electrodes and separator and behaves as a simple series resistor in the circuit. A poorly conducting cathode, for example, will have a high ohmic polarization. In the case of oxide cathodes, this can be reduced by incorporating conductive additive. This is not an issue with FeS_2, as it is a good semiconductor. Some cathodes show almost metallic behavior (e.g., CoS_2). Generally, the separator makes the largest ohmic contribution to the overall cell resistance, especially at lower temperatures when they approach the melting point of the electrolyte. Large increases in cell resistance can also occur during discharge at phase transitions in the cathode (e.g., $FeS_2 \rightarrow Li_3Fe_2S_4$).

6.1.3. Concentration polarization

Concentration gradients develop at the anode-separator and cathode separator interfaces during discharge of a cell where multi-cation electrolytes are used (e.g., LiCl–KCl eutectic) [152,153]. These gradients arise from mass-transfer limitations that can occur at each electrode as material is discharged (or charged, for secondary batteries). This resistance to mass transfer (i.e., concentration polarization) becomes increasing important at high current densities. This results in the deposition of solids from the electrolyte as the composition moves off the eutectic. This is aggravated by the tortuous paths presented by the immobilized electrolyte in the separator. This is one reason for using an all-Li^+ electrolyte when possible.

The relative performance of the pentanary and CsBr-based electrolyte are shown in Fig. 8 for Li–Si/FeS_2 single cells. The latter electrolyte cannot be used below 250 °C, which is only 24 °C above the melting point. Although it has a lower melting point, the pentanary electrolyte did not perform as well as the LiBr–KBr–CsBr electrolyte. This likely reflects higher separator impedance for the former due to the high iodide concentration. Note that the capacity of the cell is comparable to that of a Li–Si/LiCl–KCl/FeS_2 cell discharged at 400 °C but at a much higher current density of 125 mA cm^{-2}. However, that cell's total polarization of 0.2 Ω is much lower than that for the cell with the LiBr–KBr–CsBr electrolyte (~0.6 Ω) at 250 °C.

The CsBr-based ternary electrolyte has been successfully tested in battery stacks at 250 °C and a current density of

8 mA cm^{-2} for discharge times of over 32 h. Similar tests were conducted with battery stacks at 200 °C and 4 mA cm^{-2} using the pentanary electrolyte with comparable run times. However, poor reproducibility was found using the pentanary electrolyte [84]. Both of these electrolytes are compatible with FeS_2 cathodes but bromide is not stable with higher-voltage oxides cathodes, such as MnO_2, $LiMn_2O_4$, and Ag_2CrO_4 [154–156].

6.2. Nitrate-based systems

Some nitrate-based systems offer the potential of use at much lower temperatures than the best alkali halide systems because of the much lower melting points. The prominent nitrate system is the $LiNO_3$–KNO_3 eutectic with the composition 42–58 mol% [157,158]. This system was studied extensively by Miles and coworkers at the Naval Air Warfare Center (China Lake, CA). Most of the studies dealt with the basic electrochemistry; some single cells were tested but no batteries were ever built [159,160]. This electrolyte has a melting point of 124.5 °C with an ionic conductivity of 0.875 S cm^{-1} at 560 K a surface tension of 113 dynes cm^{-1}, and a viscosity of 3.497 cP at the same temperature [158]. Raistrick et al. studied the electrochemistry of LiAl anodes in this salt [161].

The conventional sulfide electrode materials are not compatible with molten nitrates, so that oxides must be used instead. Since these are typically insulators, conductive additives such as graphite must be added to the catholyte mixes—typically at a level of 10–15%. This automatically reduces the maximum energy density and specific energy that is possible. Giwa has reported the performance of the Li–Al/Ag_2CrO_4 couple in the nitrate eutectic [162,163]. More recently Guidotti and Reinhardt studied the same cathode material but with Li–Si and Li–Al anodes over a wider temperature range [164]. Other cathodes that have been examined with the eutectic nitrate electrolyte are MnO_2 [165], $LiMn_2O_4$, $LiCoO_2$, and CrO_2 [84].

A $LiNO_3$–KNO_3–$CsNO_3$ eutectic that melts at ~96 °C has been examined by Wang and Huggins [166]. They were able to discharge Li–Al/$LiCoO_2$ cells at up to 10 mA cm^{-2} at 120 °C. Using a LiCl–$LiNO_3$–$NaNO_2$ eutectic electrolyte, Bolster et al. reported discharge current densities of up to 150 mA cm^{-2} at 200 °C for Li–Al/Ag_2CrO_4 cells [167].

The compatibility of various anode materials with the molten nitrate electrolyte has also been studied [164,165]. The only reason that high-activity Li anodes can be used at all with the highly oxidizing molten nitrates is the protective passive film of Li_2O that forms on melting of the electrolyte [168]. (This is analogous to the formation of the passive LiCl film in Li/$SOCl_2$ cells.) However, this film is only stable up to a certain temperature depending on the anode material. Li–Al is more stable than Li–Si and shows an exotherm starting near 284 °C, with a major exotherm at 315 °C. In the case of the Li–Si anode, an exotherm starts near 200 °C, with a major exotherm at 260 °C as the passive film breaks down.

While single cells and heated battery stacks have been built using the nitrate electrolyte [84], the use of this technology with an internally heated thermal battery does not appear practical due to the exothermic reaction of the anode with the molten electrolyte if the passive film fails. The thermal impulse that the battery will experience at the anode-separator interface during activation will be well above the initiation temperature for exothermic reaction. (The pyrotechnic burn temperatures can exceed 1000 °C for a short period of time.) When the passive film on the anode breaks down, the resulting chemical reaction is extremely violent and would pose unacceptable hazards to nearby equipment and personnel. This can result in complete meltdown of the battery.

6.3. Chorates and perchlorates

Some work has been done studying the use of molten chlorates and perchlorates as possible battery electrolytes. $LiClO_3$, for example, melts at 128–129 °C and has been studied with Li–Al anodes at 140 °C [169]. Both chlorates and perchlorates depend on a protective passive film to prevent catastrophic reaction with highly reducing anode materials. Thus, they possess the same hazards as the molten nitrates and are not considered viable electrolyte candidates for low-temperature thermal-battery use.

6.4. Tetrachloroaluminates

Another category of low-melting molten salts is the tetracholoraluminates. The melting point of $NaAlCl_4$, for example, is 154 °C, while that for $LiAlCl_4$ is 143.5 °C. This $NaAlCl_4$ electrolyte has been used in the Na/S cells but requires a ceramic Na^+ conductor separator (e.g., β″ alumina) [170]. However, if the molten salt is placed in contact with a high-activity anode material, such as Li–Si alloy, the Al^{3+} is reduced to Al^0. The tetrachloroaluminates also have a significant vapor pressure of $AlCl_3$ at temperatures above 200 °C. In addition, they suffer from poor conductivity—only 250–500 mS cm^{-1} at 200 °C. Consequently, tetrachloroaluminates are not considered viable for possible thermal-battery applications.

6.5. Organic salts

A number of organic salts with low melting points have been examined for possible high-temperature battery use. They include acetamides, acetates, formates [171,172], urea [173], and mixtures thereof. They have limited thermal stability and all react with Li alloys when molten. In addition, they possess very low conductivities, <20 mS cm^{-1} at 150 °C for some urea mixtures [174]. While NaSCN–KSCN mixtures have been proposed as possible low-temperature electrolytes [175], similar compatibility and conductivity issues arise with their use, making them impractical for thermal-battery use [142].

Other organics that have been screened include lithium trifluoromethanesulfonimide [$LiN(CF_3SO_2)_2$ or "Li imide"; m.p. = 229.5 °C], Li trifluoromethanesulfonate [$Li(CF_3SO_3)$ or "Li triflate", m.p. = 160.8 °C], and dimethylsulfone [$(CH_3)_2SO_2$, m.p. = 108.5 °C] [142,176]. When molten, all suffered to some degree from similar incompatibilities with high-activity anodes.

There are a number of tetraalkyl ammonium salts that have reasonable low melting points that are potential candidates for

Table 10
Properties of some tetraalky ammonium and thiocyanate salts [171]

Salt	Melting point (°C)	Density (g cm^{-3})	Viscosity (cP)	Conductivity (S cm^{-1})	Temperature (°C)
$(Pr)_4NBF_4$	224.8	0.907	2.96	0.0955	257
$(Pr)_4NPF_6$	232.0	1.07	2.64	0.0773	257
$(Bu)_4NBF_4$	162.0	–	2.25	–	257
$(Bu)_4NPF_6$	247.0	0.978	2.84	0.0419	257
$(Bu)_4NBr$	119.5	1.077	–	0.00853	167
$(Bu)_4NI$	146.0	1.0769	–	0.00853	167
$(Hex)_4BF_4$	91	0.841	3.62	–	227
$(Me)_4NImide$	135 [58]	1.4 [84]	–	–	200
KSCN	172	1.55	5.09	0.311	237
NaSCN	310	–	2.56	0.754	317

low-temperature thermal batteries. Physical properties of a number of these salts are listed in Table 10. The properties of ionic liquids (electrochemical properties, density, viscosity, melting point, glass transition temperature, decomposition temperature, solubility of gas, solution in organic solvent, solvatation, ...) have been extensively reviewed by Billard and Moutiers [177]. Some of these show great promise. The tetramethylammonium imide salt, for example is stable to 300 °C in the presence of Li–Si alloy [84]. More work in this area is currently underway to explore the full potential of this category of salts. The advantage of these types of salts is that the organic cation can be easily modified by changing the functional groups to modify the salts properties to be better suited for certain low- to medium-temperature battery applications. This is not an option with conventional inorganic salts.

Except their price, which remains high compared to classical molten salts, some drawbacks are now well identified for those types of organic salts. Most of the ionic liquids (except those based on the PF_6^- anion) are stable in air and in contact with water but they are moisture sensitive, depending on their chemical structure. Experimental investigations pointed out that the basic physico-chemical properties (viscosity, density, electrochemical window, etc.) are strongly affected by the amount of water they contain [178] and many publications have stressed the importance of controlling the water amount in ionic liquids [179,180]. Various efficient procedures allow to dry ionic liquids [181–184]. Ionic liquids can be dried according an assessed procedure (drying process: heating cycle 48 h, 70 °C under vacuum) or using an innovative route: the classical freeze–thaw technique. Degassing of the ionic liquids to remove the dissolved oxygen appeared to be essential to keep the electrochemical window [185].

7. Conclusions

There are a number of physical and chemical properties of alkali-metal halide eutectics that are important for their use as molten electrolytes in conventional thermal batteries. These include density, surface tension, melting point, ionic conductivity, sensitivity towards moisture, solubility of anode and cathode materials, and composition. Data from the open literature and unpublished data have been compiled and evaluated for these properties and the results are summarized in this report. The characteristics of certain mechanical properties of separator pellets made with typical thermal-battery electrolytes are also discussed. The immobilization of the molten salt at thermal-battery operating temperatures critically depends on the nature of the oxide binder used. Control of deformation of, and electrolyte leakage from, the separator pellets is important for proper functioning of thermal batteries and factors affecting these processes are noted. These parameters are especially important for harsh battery environments that involve elevated levels of shock, spin, vibration, and acceleration.

The use of low-melting electrolytes for non-conventional thermal-battery operation was briefly described. The halide-based systems that contain iodide and/or Cs tend to have low ionic conductivities and low-rate capabilities because of unfavorable kinetics at temperatures <250 °C. Nitrate-base electrolytes have been shown to function under these conditions with the use of oxide cathodes and Li and Li-alloy anodes—sulfide cathodes are not chemically compatible. However, the breakdown of the passive Li_2O film on the anode makes these candidates hazardous to use in a real battery that may experience overheating. Similar results are noted for perchlorate and chlorate electrolytes. Many organic electrolytes (e.g., acetates, acetamides, formates, ureas), while having relatively low melting points, suffer from low ionic conductivity and, more importantly, incompatibility when molten with high-activity anodes. The tetraalkyl ammonium salts, however, do possess great potential for use in medium-temperature batteries operating at <300 °C (e.g., for borehole power supplies).

Acknowledgements

Part of this work was carried out in the frame of the thesis of P. Masset (1999–2002) who acknowledges the financial support of the CEA Le Ripault, ASB-Aerospatiale Batteries and LEPMI.

References

[1] R.A. Guidotti, P. Masset, J. Power Sources 161 (2006) 1443.
[2] A.G. Bergman, A.S. Arabadshan, Russ. J. Inorg. Chem. (English Trans.) 8 (5) (1963) 369.
[3] R.A. Guidotti, F.W. Reinhardt, Proceedings of the 33rd International Power Sources Conference, 1988, p. 369.
[4] P. Masset, PhD Thesis, National Polytechnic Institute of Grenoble, Grenoble, 2002 (in French).

[5] L. Redey, R.A. Guidotti, Proceedings of the 37th Power Sources Conference, 1996, p. 255.
[6] L. Redey, M. McParland, R. Guidotti, Proceedings of the 34th International Power Sources Conference, 1990, p. 128.
[7] C.E. Johnson, J.E. Hathaway, J. Chem. Eng. Data 14 (2) (1969) 174.
[8] Phase Diagram for Cermists, 1987.
[9] J. Sangster, A.D. Pelton, J. Phys. Chem. Ref. Data 16 (3) (1987) 509.
[10] D.B. Leiser, O.J. Whittemore Jr., J. Am. Ceram. Soc. 50 (1) (1967) 60.
[11] W. Borger, D. Kunze, H.S. Panesar, Prog. Batt. Sol. Cells 4 (1982) 258.
[12] R. Sridhar, C.E. Johnson, E.J. Cairns, J. Chem. Eng. Data 15 (2) (1970) 244.
[13] A.G. Bergman, S.I. Berezina, E.L. Bakumskaya, Russ. J. Inorg. Chem. (English Trans.) (1963) 1122.
[14] C.E. Johnson, M.S. Foster, J. Electrochem. Soc. 116 (11) (1969) 1612.
[15] C. Margheritis, G. Flor, C. Sinitri, Z. Naturforsch. A 34 (7) (1979) 836.
[16] E.J. Cairns, C.E. Crouthamel, A.K. Fisher, M.S. Foster, J.C. Hesson, C.E. Johnson, H. Shimatoke, A.D. Tavegaugh, U.A. At. Energy Comm. Report ANL 7316, 1967.
[17] C.E. Johnson, E.J. Hathaway, J. Electrochem. Soc. 118 (4) (1971) 631.
[18] C. Margheritas, G. Flor, S. Sinistri, Z. Naturforsch. A 20 (6/7) (1975) 896.
[19] J.R. Selman, D.K. DeNuccio, C.J. Sy, R.K. Steunenberg, J. Electrochem. Soc. 124 (8) (1977) 1160.
[20] T. Kaun, J. Electrochem. Soc. 132 (12) (1985) 3063.
[21] T. Kaun, Proceedings of the Joint International Symposium on Molten Salts, 1987, p. 621.
[22] D.R. Vissers, L. Redey, T. Kaun, J. Power Sources 26 (1989) 37.
[23] H. Ohno, H. Shimotake, New Mater. New Process. 2 (1983) 283.
[24] N.P. Yao, J. Electrochem. Soc. 119 (8) (1971) 1056.
[25] E.J. Cairns, R.K. Steunenberg, High-temperature batteries, in: C. Rouse (Ed.), Progress in High Temperature Physics and Chemistry, New York, 1973. p. 63.
[26] JANAF Thermochemical Tables, 2nd ed., D.R. Stull, H. Prophet (Eds.), National Standards Reference Data Series, NSRDS-NBS 37, June 1971.
[27] J.A. Plambeck, Encyclopedia of Electrochemistry of Elements, vol. X, Ed. Marcel Dekker Inc., 1976.
[28] J. Sangster, J. Phase Equilibria (1990).
[29] C.E. Vallet, D.E. Heatherly, J.R. Heatherly, J. Braunstein, J. Electrochem. Soc. 130 (12) (1983) 2370.
[30] J. Braunstein, C.E. Vallet, J. Electrochem. Soc. 126 (6) (1979) 960.
[31] JANAF Thermochemical Tables, 2nd ed., D.R. Stull, H. Prophet (Eds.), National Standards Reference Data Series, NSRDS-NBS 37, June 1971.
[32] J.A. Plambeck, Encyclopedia of Electrochemistry of Elements, vol. X, Ed. Marcel Dekker Inc., 1976.
[33] P. Masset, J. Power Sources 160 (1) (2006) 688.
[34] J.R. Birk, R.K. Steunenberg, New use of sulfur, in Advances in Chemistry, Series 140, ACS, J.R.W. Editor, 1975.
[35] Y. Kansaki, T. Takahashi, J. Electroanal. Interf. Electrochem. 58 (1975) 339.
[36] Y. Kansaki, T. Takahashi, J. Electroanal. Interf. Electrochem. 58 (1975) 349.
[37] P. Bonhôte, A. Dias, P. Papageorgiou, N. Kalyanasundaram, K. Graetzel, Inorg. Chem. 35 (1996) 1168.
[38] V.V. Kharton, F.M.B. Marques, A. Atkinson, Solid State Ionics 174 (2004) 135.
[39] P. Masset, A. Henry, J.-Y. Poinso, J.-C. Poignet, J. Power Sources 160 (1) (2006) 752.
[40] R.C. Vogel, L. Burris, A.V. Tavegaugh, D.S. Webster, E.R. Proud, Argonne National Laboratories, Report ANL-7775, 1970, p. 135.
[41] G.J. Janz, NIST Standard Reference Database 27: Properties of Molten Salts Database. Single Salts and Salt Mixtures Data; Density, Viscosity, Electrical Conductance, and Surface Tension, ver. 20, 1992.
[42] J. Schenin-King, PhD Thesis, University Paris 6, 1994 (in French).
[43] V.L. Cherignets, Electrochim. Acta 42 (23/24) (1997) 3619.
[44] L. Redey, M. McParland, R. Guidotti, Proceedings of the 34th International Power Sources Conference, 1990, p. 128.
[45] F.M. Delnick, R.A. Guidotti, J. Electrochem. Soc. 137 (1) (1990) 11.
[46] F.L. Tye, J. Power Sources 9 (1963) 89.
[47] J. Newman, W. Tiedemann, AIChE J. 21 (3) (1975) 25.
[48] L. Sigrist, O. Dossenbach, N. Ibl, J. Appl. Electrochem. 10 (1980) 223.
[49] P. Masset, S. Schoeffert, J.Y. Poinso, J.-C. Poignet, J. Power Sources 139 (2005) 356.
[50] E.R. Van Arstdalen, I.S. Yaffe, J. Phys. Chem. 59 (1955) 118.
[51] R.A. Guidotti, F.W. Reinhardt, E.V. Thomas, Sandia National Laboratories report SAND90-2318, May, 1995.
[52] R.A. Guidotti, F.W. Reinhardt, Sandia National Laboratories report SAND90-2103, 1991.
[53] G.J. Janz, R.P.T. Tomkins, C.B. Allen, J.R. Downey, S.K. Singer, J. Phys. Chem. Ref. Data 6 (3) (1977) 516.
[54] A.W. Adamson, Physical Chemistry of Surfaces, 3rd ed., John Wiley and Sons, New York, 1976, pp. 333–371.
[55] A.W. Kingery, H.K. Bowen, D.R. Uhlmann, Introduction to Ceramics, 2nd ed., John Wiley and Sons, New York, 1976, pp. 177–216.
[56] G.J. Janz, R.P.T. Tomkins, C.B. Allen, J.R. Downey, G.E. Gardner, U. Krebs, S.K. Singer, J. Phys. Chem. Ref. Data 4 (3) (1975) 1045.
[57] G.J. Janz, R.P.T. Tomkins, C.B. Allen, J.R. Downey, G.E. Gardner, U. Krebs, S.K. Singer, J. Phys. Chem. Ref. Data 4 (3) (1975) 1049.
[58] J.G. Eberhart, Report Argonne National Laboratories, ANL79-34, 1979.
[59] G.K. Johnson, et al., in: B. Mishra, W.A. Aerill (Eds.), Warrendale, The Minerals, Metals & Material Society, PA, 1994, p. 199.
[60] K. Gourishankar, E.J. Karell, Light Met. (1999) 1123.
[61] K. Gourishankar, L. Redey, M. Williamson, Light Met. (2002) 1075.
[62] N.M. Barbin, V.N. Nekkrasov, Electrochim. Acta 44 (199) (2006) 4479.
[63] Y. Kaneko, H. Kojima, Denki Kagaki 42 (1974) 304.
[64] R.A. Guidotti, F.W. Reinhardt, J. Power Sources 15 (1995) 443.
[65] P. Masset, S. Schoeffert, J.Y. Poinso, J.C. Poignet, J. Power Sources 137 (2004) 140.
[66] W.F. Linke, Solub. Inorg. Metall. Org. Compd. 2 (1965).
[67] I. Ikeuchi, C. Krohn, Acta Chem. Scand. 23 (1969) 2230.
[68] I.-M. Chou, S.M. Sterner, K.S. Pitzer, Geochim. Cosmochim. Acta 56 (1992) 2281.
[69] D. Zeng, PhD Thesis, Technical University of Bergakademie Freiberg, Germany, 2003 (in German).
[70] M. Manewa, H.P. Fritz, A. Anorg. Allg. Chem. 296 (3) (1973) 279.
[71] G.F. Huttig, W. Steudemann, Z. Phys. Chem. 126 (1/2) (1927) 279.
[72] W. Voigt, D. Zeng, Pure Appl. Chem. 74 (10) (2002) 1909.
[73] K. Rudo, P. Hartwig, W. Weppner, Rev. Chim. Miner. 17 (4) (1980) 420.
[74] B. Chevalier, CNAM report (Electrochemistry), 1988, p. 12 (in French).
[75] M.A. Clynne, R.W. Potter II, J. Chem. Eng. Data 24 (1979) 338.
[76] T. Fanghänel, K. Kravchuk, W. Voigt, H.-H. Emons, Z. Anorg. Allg. Chem. 547 (1987) 21.
[77] M.A. Urusova, V.M. Valyashko, Zh. Neorg. Khim. 28 (1983) 1845.
[78] E. Strauss, G. Ardel, V. Livshits, L. Burstein, D. Golodnitsky, E. Peled, J. Power Sources 88 (2000) 206.
[79] M.E. Melnichak, J.O. Kleppa, J. Chem. Phys. 52 (4) (1970) 1790.
[80] P. Hartwig, A. Rabenau, W. Weppner, J. Less-Common Met. 78 (2) (1981) 227.
[81] B. Schoch, A. Rabenau, W. Weppner, H. Hahn, Z. Anorg. Allg. Chem. 518 (1984) 137.
[82] R. Parash, F. Broitman, U. Mor, D. Ozer, A. Bettelheim, J. Electrochem. Soc. 131 (11) (1984) 2531.
[83] G.M. Unshakov, Dokl. Akad. Nauk SSSR 87 (5) (1952) 791.
[84] R.A. Guidotti, Sandia National Laboratories, unpublished data, 2002.
[85] R.B. Swaroop, J.E. Battles, J. Electrochem. Soc. 128 (9) (1981) 1873.
[86] G. Bandyopadhyay, R.B. Swaroop, J.E. Battles, J. Electrochem. Soc. 129 (10) (1982) 2187.
[87] D.M. Bush, Sandia National Laboratories report SC-RR-66-202, 1996.
[88] R.A. Guidotti, F.W. Reinhardt, Sandia National Laboratories report SAND90-2104, 1996.
[89] R.A. Guidotti, F.W. Reinhardt, E.V. Thomas, Proceedings of the 39th Power Sources Conference, 2000, p. 478.
[90] R.A. Guidotti, F.W. Reinhardt, A.H. Andazola, SAND2002-1458, June 2002.
[91] J.A. Plambeck, J.P. Elder, H.A. Laitinen, J. Electrochem. Soc. 113 (1966) 931.

[92] J.J. Warren, Jr., in: G. Mamamtov, R. Marassi (Eds.), Molten Salts Chemistry (1987) 237.
[93] A.S. Dworkin, H.R. Bronstein, M.A. Bredig, J. Phys. Chem. 66 (1962) 572.
[94] M.V. Smirnov, N.P. Podlesnyak, Zhurhal Prikladnoi Khimii 43 (7) (1970) 1463.
[95] J. Liu, PhD Thesis, National Polytechnic Institute of Grenoble, Grenoble, 1988 (in French).
[96] T. Nakajima, Bull. Chem. Soc. Jap. 47 (8) (1974) 2071.
[97] R.J. Heus, J. Egan, J. Phys. Chem. 77 (16) (1989) 1989.
[98] G.M. Haarberg, K.S. Osen, J.J. Egan, H. Heyer, W. Freyland, Ber. Bunsenges. Phys. Chem. 92 (1988) 139.
[99] G.M. Haarberg, K.S. Osen, R.J. Heus, J.J. Egan, J. Electrochem. Soc. 137 (9) (1990) 2777.
[100] M. Okada, R.A. Guidotti, J.D. Corbett, Inorg. Chem. 7 (1968) 2115.
[101] J. Liu, J.-C. Poignet, J. Appl. Electrochem. 22 (1992) 1110.
[102] J. Liu, J.-C. Poignet, J. Appl. Electrochem. 20 (1990) 864.
[103] P. Hebant, G.S. Picard, Electrochim. Acta 43 (14/15) (1998) 2071.
[104] G.J. Reynolds, M.C.Y. Lee, R.A. Huggins, Proceedings of the Fourth International Symposium on Molten Salts, May 1983, 1983.
[105] R.J. Heus, J.J. Egan, Proceedings of the International Symposium on Molten Salts, The Electrochemical Society, Pennington, NJ, 1976, p. 523.
[106] L. Redey, Private communication, 1993.
[107] L. Redey, S.L. Marshall, Extended Abstracts, vol. 89-1, The Electrochemical Society, Pennington, NJ, 1989, p. 27 (Proceedings of the 175th Meeting of The Electrochemical Society, May 7–12, 1989, Los Angeles, CA).
[108] R. Knödler, J. Electrochem. Soc. 130 (1) (1983) 16.
[109] R.N. Snyder, J.J. Lander, J. Electrochem. Soc. 4 (3/4) (1966) 179.
[110] R.C. Sharma, Y.A. Chang, Met. Trans. B 10 (1979) 103.
[111] W. Burgmann, G. Urbain, M.G. Frohberg, Mem. Sci. Rev. Metall. 65 (7/8) (1968) 567.
[112] S. Dallek, B.F. Larrick, Thermochim. Acta 95 (1985) 139.
[113] J.P. Pemsler, R.K.F. Lam, J.K. Litchfield, S. Dallek, B.F. Larrick, B.C. Beard, J. Electrochem. Soc. 137 (1) (1990) 1.
[114] G. Barlow, Final Report to Lawrence Berkeley Laboratory, December 1986.
[115] P. Masset, V. Frotté, J.-Y. Poinso, J.-C. Poignet, J. Power Sources, in preparation.
[116] M.C. Hash, J.A. Smaga, R.A. Guidotti, F.W. Reinhardt, Proceeding of Eighth International Symposium on Molten Salts, 1992, p. 228.
[117] R.A. Guidotti, F.W. Reinhardt, J.A. Smaga, Proceedings of the 34th International Power Sources Symposium, 1990, p. 132.
[118] L. Redey, J.A. Smaga, J.E. Battles, R.A. Guidotti, Argonne National Laboratory report ANL-87-6, 1987.
[119] C.H. Liu, A.J. Zielen, D.M. Gruen, J. Electrochem. Soc. 120 (1) (1973) 14.
[120] J. Phillips, H.F. Gibbard, Proceedings of the Second International Symposium Molten, Electrochem. Soc. Pennington, NJ, 81-10, 1980, p. 45.
[121] D. Warin, Z. Tomczuk, D.R. Vissers, J. Electrochem. Soc. 130 (1) (1983) 64.
[122] S. Sharma, J. Electrochem. Soc. 133 (5) (1986) 859.
[123] M.L. Saboungi, J.J. Marr, M. Blander, J. Electrochem. Soc. 125 (10) (1978) 1567.
[124] M.L. Saboungi, J.J. Marr, M. Blander, Met. Trans. B 10 (1979) 477.
[125] R.A. Sharma, R.N. Seefurth, J. Electrochem. Soc 131 (5) (1984) 1084.
[126] R.N. Seefurth, S. Sharma, J. Electrochem. Soc. 135 (4) (1988) 796.
[127] Z. Tomczuk, D.R. Vissers, M.L. Saboungi, Proceedings of Fourth International Symposium on Molten Salts, vol. 84-2, The Electrochemical Society, 1984, p. 352.
[128] G. Santarini, C.R. Acad. Sc. Paris, Série C T287 (1979) 421.
[129] G. Santarini, Electrochim. Acta 27 (4) (1982) 495.
[130] Z. Tomczuk, B. Tani, N.C. Otto, M.F. Roche, D.R. Vissers, J. Electrochem. Soc. 129 (5) (1982) 925.
[131] Z. Tomczuk, S.K. Preto, M.F. Roche, J. Electrochem. Soc. 128 (4) (1981) 760.
[132] S.K. Preto, Z. Tomczuk, S. von Winbush, M.F. Roche, J. Electrochem. Soc. 130 (2) (1983) 264.
[133] K. Grjotheim, B. Haugsdal, H. Kvande, H.G. Nebell, T.A. Utigard, J. Electrochem. Soc. 135 (1) (1988) 51.
[134] W. Giggenbach, Inorg. Chem. 10 (1971) 1308.
[135] R. Schieck, A. Hartmann, S. Fiechter, R. Könenkamp, H. Wetzel, J. Mater. Res. 5 (7) (1990) 1567.
[136] J.A. Tossell, D.J. Vaughan, J.K. Burdett, Phys. Chem. Miner. 7 (4) (1981) 177.
[137] D.M. Gruen, R.L. McBeth, A.J. Zielen, J. Am. Ceram. Soc. 93 (24) (1971) 6691.
[138] R.A. Guidotti, F.W. Reinhardt, J.G. Odinek, J. Power Sources 136 (2) (2004) 257.
[139] R.A. Guidotti, F.W. Reinhardt, Proceedings of the International Symposium on Molten Salts XII, vol. 99-41, 2000, p. 451.
[140] R.A. Guidotti, F.W. Reinhardt, Proceedings of the International Symposium on Molten Salts XII, vol. 99-41, 2006, p. 701.
[141] R.A. Guidotti, F.W. Reinhardt, Proceedings of the 36th IECEC, vol. 1, 2001, p. 905.
[142] R.A. S Guidotti, Proceedings of the 35th IECEC Meeting, vol. 2, 2000, p. 1276.
[143] R.A. Guidotti, F.W. Reinhardt, Proceedings of the 39th Power Sources Conference, 2000, p. 470.
[144] R.A. Normann, R.A. Guidotti, Trans. Geotherm. Resour. Council 20 (1996) 509.
[145] G.J. Janz, R.P.T. Tomkins, C.B. Allen, J.R. Downey, S.K. Singer, J. Phys. Chem. Ref. Data 6 (3) (1977) 516.
[146] G.J. Janz, R.P.T. Tomkins, C.B. Allen, J.R. Downey, S.K. Singer, J. Phys. Chem. Ref. Data 6 (3) (1977) 485.
[147] G.J. Janz, R.P.T. Tomkins, C.B. Allen, J.R. Downey, S.K. Singer, J. Phys. Chem. Ref. Data 6 (3) (1977) 564.
[148] D.L. Thomas, J.-Y. Cherng, D.N. Bennion, J. Electrochem. Soc. 135 (11) (1988) 2674.
[149] G.G. Diogenov, V.I. Ermachkov, Russ. J. Inorg. Chem. 12 (3) (1967) 436.
[150] B. Codd, Proceedings of the 33rd Power Sources Conference, 1988, p. 359.
[151] R.A. Guidotti, F.W. Reinhardt, Proceedings of the Electrochemical Society 2002-19 (Molten Salts XIII), 2002, p. 63.
[152] C.E. Vallet, L.M. Kidd, D.E. Murphy, R.L. Sherman, J. Braunstein, J. Electrochem. Soc. 129 (5) (1982) 931.
[153] C.E. Vallet, D.E. Heatherly, R.L. Sherman, J. Braunstein, J. Electrochem. Soc. 129 (1) (1982) 49.
[154] R.A. Guidotti, F.W. Reinhardt, Proceedings of the 39th Power Sources Conference, 2000, p. 470.
[155] R.A. Guidotti, F.W. S Reinhardt, Proceedings of the International Symposium on Molten Salts XII, vol. 99-41, 2000, p. 451.
[156] R.A. Guidotti, F.W. Reinhardt, New Technol. Med. 2 (1) (2001) 26.
[157] X. Zhang, K. Xu, Y. Gao, Thermochim. Acta 385 (2002) 81.
[158] G.J. Janz, U. Krebs, N.F. Siegenthaler, R.P.T. Tomkins, J. Phys. Chem. Ref. Data 1 (3) (1972) 671.
[159] M.H. Miles, Proceedings of the 39th International Power Sources Conference, 2000, p. 560.
[160] M.H. Miles, Proceedings of the 14th Annual Battery Conference, 1999, p. 39.
[161] I.D. Raistrick, J. Poris, R.A. Huggins, in: H.Y. Venkatasetty (Ed.), Proceedings of the Symposium on Lithium Batteries, vol. 81-4, The Electrochemical Society, Pennington, NJ, 1981, p. 477.
[162] C.O. Giwa, Proceedings of the 35th International Power Sources Symposium, 1992, p. 215.
[163] C.O. Giwa, Mater. Sci. Forum 73–75 (1991) 699.
[164] R.A. Guidotti, F.W. S Reinhardt, Proceedings of the 198th Meeting of The Electrochemical Society, Phoenix, AZ, October 22–27, 2000.
[165] R.A. Guidotti, F.W. Reinhardt, Proceedings of the 41st Power Sources Conference, 2004, p. 141.
[166] J. Wang, R.A. Huggins, Proceedings of the Electrochemical Society, vol. 84-4, 1983, p. 64.
[167] M.-E. Bolster, J. Embrey, J. Foxwell, R.J. Staniewicz, Extended Abstracts of the Fall Meeting of The Electrochemical Society, vol. 89-2, 1989, p. 147.

[168] M.H. Miles, G.E. McManis, A.N. Fletcher, Electrochim. Acta 30 (1985) 889.
[169] D.H. Shen, D.N. Bennion, Technical Report #2, Office of Naval Research, Contract No. N0014-80-C-0345, January, 1981.
[170] J. Caja, D. Dunstan, G. Mamantov, in: T. Keily, B.W. Baxter (Eds.), Proceedings of the 17th International Power Sources Symposium on Power Sources, vol. 13, Bournemouth, April, 1991, 1991, p. 333.
[171] G.J. Janz, F.W. Dampier, G.R. Lakshminarayan, P.K. Lorenz, R.P.T. Tomkins, National Standard References Data Series, National Bureau of Standards 15 (NSRDS-NBS 15), 1968, 100–105.
[172] R.A. Wallace, P.F. Bruins, J. Electrochem. Soc. 114 (3) (1967) 209.
[173] R.A. Wallace, P.F. Bruins, J. Electrochem. Soc. 114 (3) (1967) 212.
[174] Q. Yang, D. Zhu, G. Liu, S. Ke, Y. Tong, L. Sha, Proceedings of the 11th International Symposium on Molten Salts, 1998, p. 18.
[175] R.E. Panzer, U.S. Patent, 3,367,800, February 6, 1968.
[176] C.O. Giwa, Proceedings of the 36th Power Sources Conference, 1994, p. 325.
[177] I. Billard, G. Moutiers, Techniques de l'Ingénieur, AF 6712, 2005 (in French).
[178] K.R. Seddon, A. Stark, M.J. Torres, Pure Appl. Chem. 72 (2000) 2275.
[179] C.D. Tran, S.H. De Paoli Lacerda, D. Oliveira, Appl. Spectrosc. 57 (2003) 152.
[180] L. Cammarata, S.G. Kazarian, P.A. Salter, T. Welton, Phys. Chem. Chem. Phys. 3 (2001) 5192.
[181] I. Billard, S. Mekki, C. Gaillard, P. Hesemann, G. Moutiers, C. Mariet, A. Labet, J.C.G. Bünzli, Eur. J. Inorg. Chem. 6 (2004) 1190.
[182] J.D. Holbrey, K.R. Seddon, J. Chem. Soc., Dalton Trans. 2133 (1999).
[183] C.M. Gordon, J.D. Holbrey, A.R. Kennedy, K.R. Seddon, J. Mater. Chem. 8 (1998) 2627.
[184] B.K. Sweeny, D.G. Peters, Electrochem. Commun. 3 (2001) 712.
[185] Y. Katayama, H. Onodera, M. Yamagata, T. Miura, J. Electrochem. Soc. 151 (2004) A59.